ACS NANO

www.acsnano.org

ARTICLE

Graphene as Thinnest Coating on Copper Electrodes in Microbial Methanol Fuel Cells

Jamil Islam, Parthiba Karthikeyan Obulisamy, Venkata K.K. Upadhyayula, Alan B. Dalton, Pulickel M. Ajayan,* Muhammad M. Rahman,* Manoj Tripathi,* Rajesh Kumar Sani,* and Venkataramana Gadhamshetty*

Cite This: *ACS Nano* 2023, 17, 137−145

Read Online

ACCESS | Metrics & More | Article Recommendations | Supporting Information

ABSTRACT: **Dehydrogenation of methanol (CH_3OH) into direct current (DC) in fuel cells can be a potential energy conversion technology. However, their development is currently hampered by the high cost of electrocatalysts based on platinum and palladium, slow kinetics, the formation of carbon monoxide intermediates, and the requirement for high temperatures. Here, we report the use of graphene layers (GL) for generating DC electricity from microbially driven methanol dehydrogenation on underlying copper (Cu) surfaces. Genetically tractable *Rhodobacter sphaeroides* 2.4.1 (Rsp), a nonarchetypical methylotroph, was used for dehydrogenating methanol at the GL-Cu surfaces. We use electrochemical methods, microscopy, and spectroscopy methods to assess the effects of GL on methanol dehydrogenation by Rsp cells. The GL-Cu offers a 5-fold higher power density and 4-fold higher current density compared to bare Cu. The GL lowers charge transfer resistance to methanol dehydrogenation by 4 orders of magnitude by mitigating issues related to pitting corrosion of underlying Cu surfaces. The presented approach for catalyst-free methanol dehydrogenation on copper electrodes can improve the overall sustainability of fuel cell technologies.**

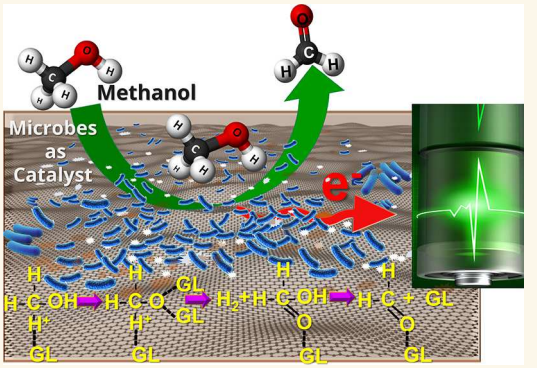

KEYWORDS: *graphene, microbial corrosion, surface science, methylotrophs, methanol dehydrogenation*

Methanol fuel cells (CH_3OH-FCs) offer ease of fuel handling, low thermal signatures, and an eco-friendly power source compared to competing fuel cell (FC) technologies. They support marine vessels (e.g., submarines), portable electronics, military bases,[1−8] mobile applications (e.g., electric vehicles),[9] telecommunications towers, and data centers.[10] Generally, discarded methane gases can be converted into CH_3OH for subsequent use in CH_3OH-FCs. A goal of developing viable CH_3OH-FC technologies aligns with the National Academy of Engineering's priority of reducing greenhouse gas emissions.[11] The global market for direct CH_3OH-FCs has been predicted to reach ~$288 M by 2027.[12] Given these potential benefits, federal agencies, including the U.S. Department of Energy, have identified key challenges facing CH_3OH-FC technologies.[13] An immediate priority is to develop alternatives to expensive catalysts for reducing overpotential to CH_3OH dehydrogenation (e.g., platinum (Pt),[14] palladium (Pd), Pt−Sn,[15] Pd−Sn, Pd−cobalt−gold, and Pt−ruthenium[16]). Living microorganisms, especially methylotrophs ("methanol oxidizing bacteria"), have the potential to replace these chemical catalysts.[17] They contain inherent enzymes (e.g., methanol dehydrogenase) that can dehydrogenate CH_3OH[18] and liberate reducing equivalents that can be used to generate direct current (DC) electricity in fuel cells.

Copper (Cu) electrodes may serve as promising candidates for obtaining high-performance CH_3OH-FCs.[19] Cu electrodes are desirable in terms of low cost ($9.30/kg),[20] malleability,[21−23] high tensile strength (210 MPa), and electrical conductivity (58.7×10^6 S/m),[24] especially when compared to carbonaceous electrode materials. For example, the electrical conductivity of Cu is nearly 900-fold higher than polycrystalline graphite materials. Furthermore, Cu surfaces have been reported to dehydrogenate aqueous CH_3OH[25] into simpler products such as formaldehyde and carbon dioxide. However, methanol dehydrogenation on polycrystalline Cu surfaces

Received: June 5, 2022
Accepted: December 12, 2022
Published: December 19, 2022

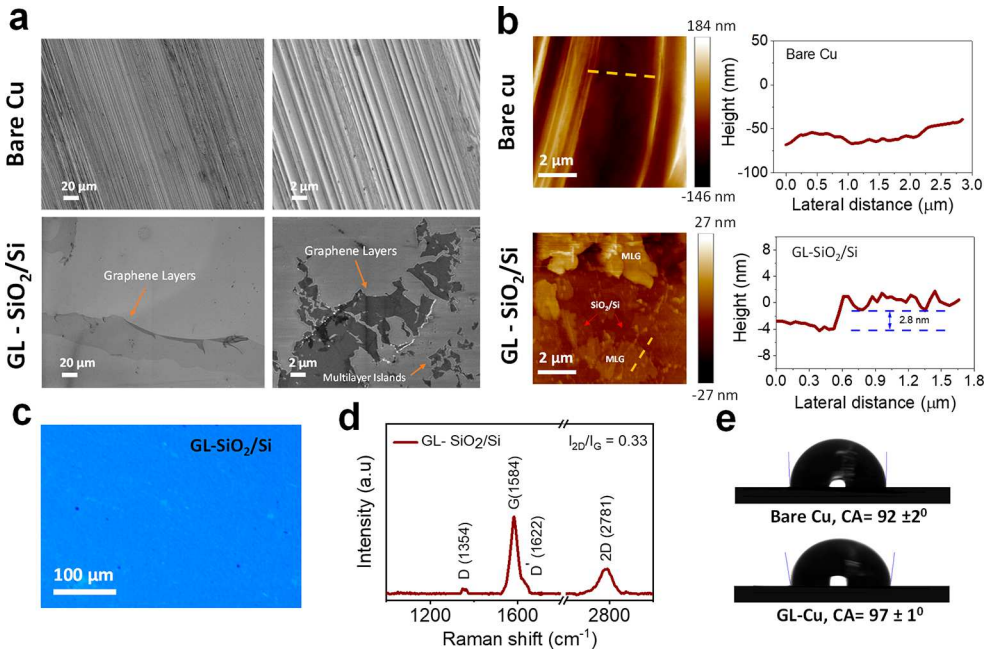

Figure 1. Characterization of atomic graphene layers. (a) SEM images of bare Cu and graphene layers (GL) used to modify the Cu substrate (shown on SiO_2/Si substrate). (b) Atomic force microscope (AFM) images of Cu and GL-SiO_2/Si and corresponding height profiles. (c) Optical images of the transferred GL films on SiO_2/Si (background color). (d) Corresponding Raman spectra of the transferred GL on SiO_2/Si. GL displays a sharp G band (~1584 cm^{-1}) and 2D band (~2781 cm^{-1}). (e) Static water contact angle values for Cu and GL-Cu.

requires elevated temperatures (>400 °C) and extremely low pressures (0.6 mbar).[26] Although single Cu (111) crystals dehydrogenate methanol at ambient temperatures (25 °C), they still require low pressures (0.5 mTorr).[27] Single Cu crystals are also disadvantageous in terms of high cost and low strength.

There is a need to develop viable strategies for enabling catalyst-free CH_3OH dehydrogenation on Cu surfaces under ambient conditions. It is important for such Cu electrodes to resist corrosion.[28] To address these concerns, the current study explores the use of graphene as a minimally invasive coating for enabling methanol biotransformation on Cu electrodes in CH_3OH-FCs.[29] Graphene coatings offer diverse advantages, including barrier properties, high electrical conductivity, and low-profile thickness, while serving as excellent supports for promoting tunable electrochemical interactions with the supported biocatalysts. Such coatings can decrease charge transfer resistance to CH_3OH, improve the electron transfer rate, and enhance performance of the fuel cell.[30] The bare metal electrodes in fuel cells experience enormous surface oxidation or corrosion, leading to frequent deactivation through direct exposure to chemical reactants.[22,31−33] Graphene over the metallic substrate (such as Cu) alters its electroneutrality through the modulation in the Fermi level (E_F). Thus, coverage of impermeable graphene resists corrosion, supports microbial growth, and simultaneously sustains electrochemical current responsible for improved catalytic activity, all without impeding the functionality of the underlying metal electrodes.[34] Also, the presence of a graphene layer offers charged active regions through the generation of polarized sites (wrinkles and grain boundaries in metal grains). As a result, these positively charged sites may favor the adsorption of active species for dehydrogenation of methanol.[35]

Unlike prior electrochemical studies (discussed in ref 30)[36] that used dopants (e.g., N, S, and B) for modifying graphene, we use pristine graphene layers for biologically dehydrogenating CH_3OH on Cu surfaces. A genetically tractable *Rhodobacter sphaeroides* (Rsp), a nonarchetype methylotroph,[37−39] was used as a biocatalyst. Our results confirm that graphene layers form a minimally invasive coating on Cu to increase power density and current density by 5 orders and 4 orders of magnitude, respectively, compared to bare Cu. A series of electrochemical, imaging, and spectroscopy methods were used to discern the underlying phenomena that enabled CH_3OH dehydrogenation by Rsp cells at the Gr−Cu interfaces.

RESULTS AND DISCUSSION

Characterization of Pristine Graphene Layers. We synthesized graphene layers (GL) on 25-μm-thick Cu foils using typical chemical vapor deposition (CVD) growth parameters (35 sccm CH_4, 1000 °C, 500 mTorr). A CH_4/H_2 mixture (10:30 sccm) was introduced at 940 °C for 20 min at atmospheric pressure. Conformality of graphene on Cu foil was established in the form of wrinkles across the grain boundaries (SEM image, Figure 1a). For characterizing the layers, the graphene film from the Cu foil was transferred onto SiO_2/Si substrate using a poly(methyl methacrylate) (PMMA) transfer method described in our earlier studies.[40,41] Noncontact mode AFM techniques were used to study the surface morphology of the graphene films on SiO_2/Si (Figure 1b). The thickness of the film was ~2.8 nm, which translates to eighr GLs based on the layer thickness of 0.34 nm as calculated using empirical force-constant models.[42,43] The GL samples displayed a varying film thickness, evident from light blue within the bright blue region (Figure 1c). The G and 2D bands corresponding to E_{2g} vibration modes at 1584 and A_{1g} vibration modes at 2781 cm^{-1}, respectively, in the Raman

https://doi.org/10.1021/acsnano.2c05512
ACS Nano 2023, 17, 137−145

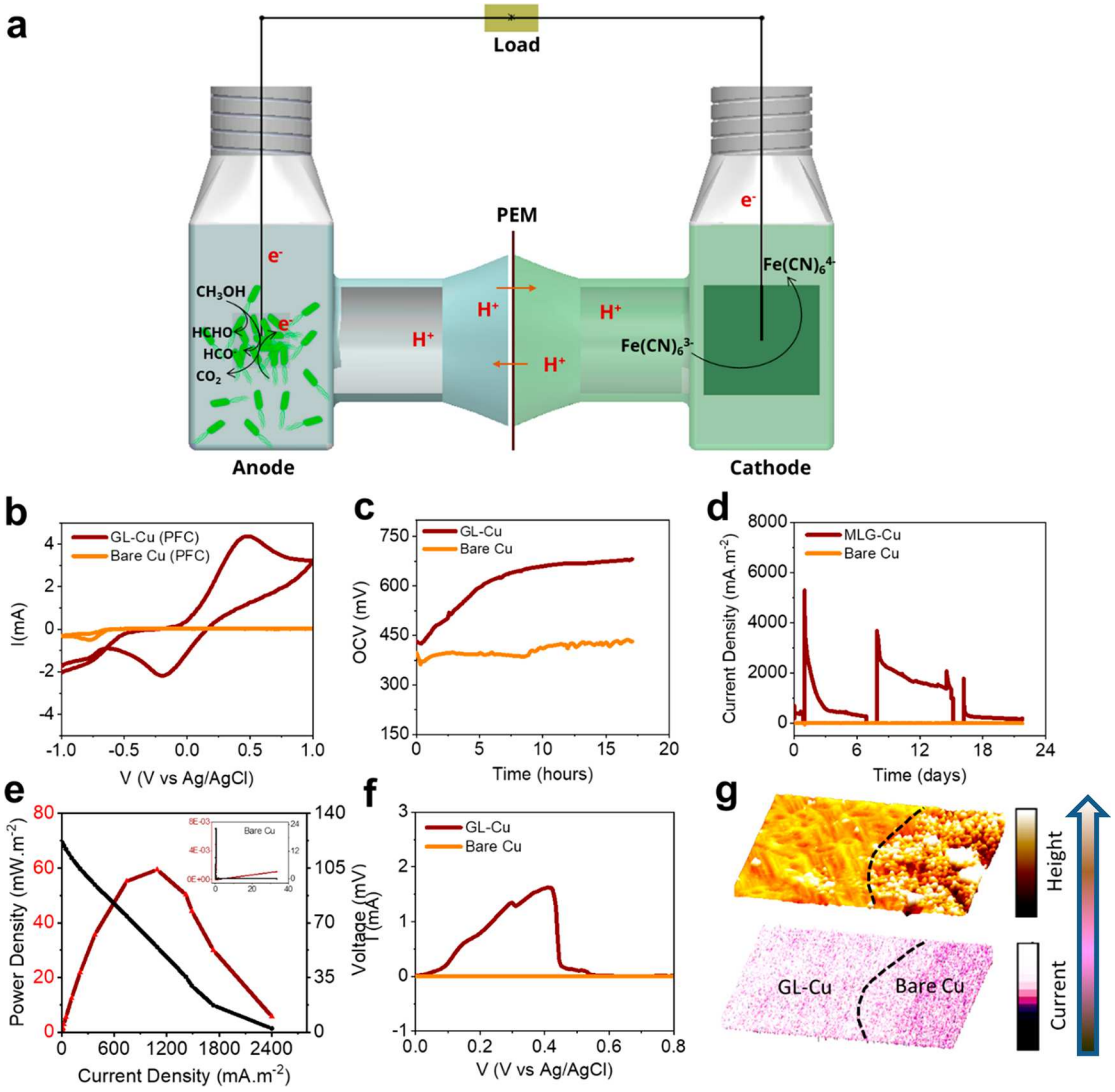

Figure 2. Bioelectrocatalytic performance of GL-Cu compared to bare Cu. (a) An illustration of CH_3OH-FCs with GL-Cu (Rsp cells) in the anode and a carbon cloth cathode (50 mM ferricyanide) separated by a proton exchange membrane (PEM). (b) Cyclic voltammogram of GL-Cu and bare Cu in 10 mM potassium ferricyanide in a three-electrode system. Temporal performance of GL-Cu and bare Cu in CH_3OH-FCs: (c) OCV, (d) current density, (e) power density, (f) LSV plots for CH_3OH dehydrogenation on day 7, and (g) AFM topography and current map of GL-Cu and bare Cu. The bright region indicates higher topography and current. The reduced conductivity of the bare Cu surface is due to the formation of oxide layers. The dashed line represents the interface between bare Cu and that coated with GL.

spectra confirmed the signatures of graphene (Figure 1d). A D band (1354 cm^{-1}) indicated the presence of inherent defects.[44,45] The I_{2D}/I_G ratio of 0.33 further confirmed multiple layers of graphene. The Raman signatures of as-grown GL on Cu (GL-Cu) were compared with the transferred samples (GL-Si-SiO_2; see Figure S1). The transferred samples displayed inferior quality compared to GL-Cu samples. This can be attributed to the presence of the organic residue (PMMA) and unwanted folds and wrinkles generated during the PMMA-mediated method. The intensity of the D band was used to locate the interfacial grain boundaries (GB) over the GL-Cu surface, while a shift in the position of G and 2D bands was used to evaluate the physical straining and carrier concentration, respectively.[46] GB displayed peculiar characteristics in terms of relatively higher carrier concentration and compression of C−C bonds than the surrounding grain regions (see Figure S2). These characteristics were further validated by exposing the GBs to pure methanol for different intervals (3 and 24 h). Under these exposure conditions, we observed the significant upshift in the G peak position at the GB compared to the grain regions, while the 2D peak position remained consistent. This result indicates the efficient decrease in carrier concentration of charges at GB. The drop shape contact angles using water for bare Cu and GL-Cu (Figure 1e) were measured as 92° ± 2.0° and 97° ± 1.0°, respectively.[41,47] These differences in hydrophobicity were further validated through high-resolution force−distance spectroscopy in terms of the pull-out force against the hydrophilic tip apex. The higher the pull-out force (nN) value, the higher the adhesion force (see Figure S3c). The transferred-graphene films that were used to modify glassy carbon electrodes also consisted of multiple layers of graphene (see Figure S3a,b).

High-Performance Graphene Layers on Cu Electrodes for CH_3OH-FCs. An immediate application of as-grown conformal graphene layers is to enable the use of underlying Cu as an anode in CH_3OH-FC (modeled in a two-

https://doi.org/10.1021/acsnano.2c05512
ACS Nano 2023, 17, 137−145

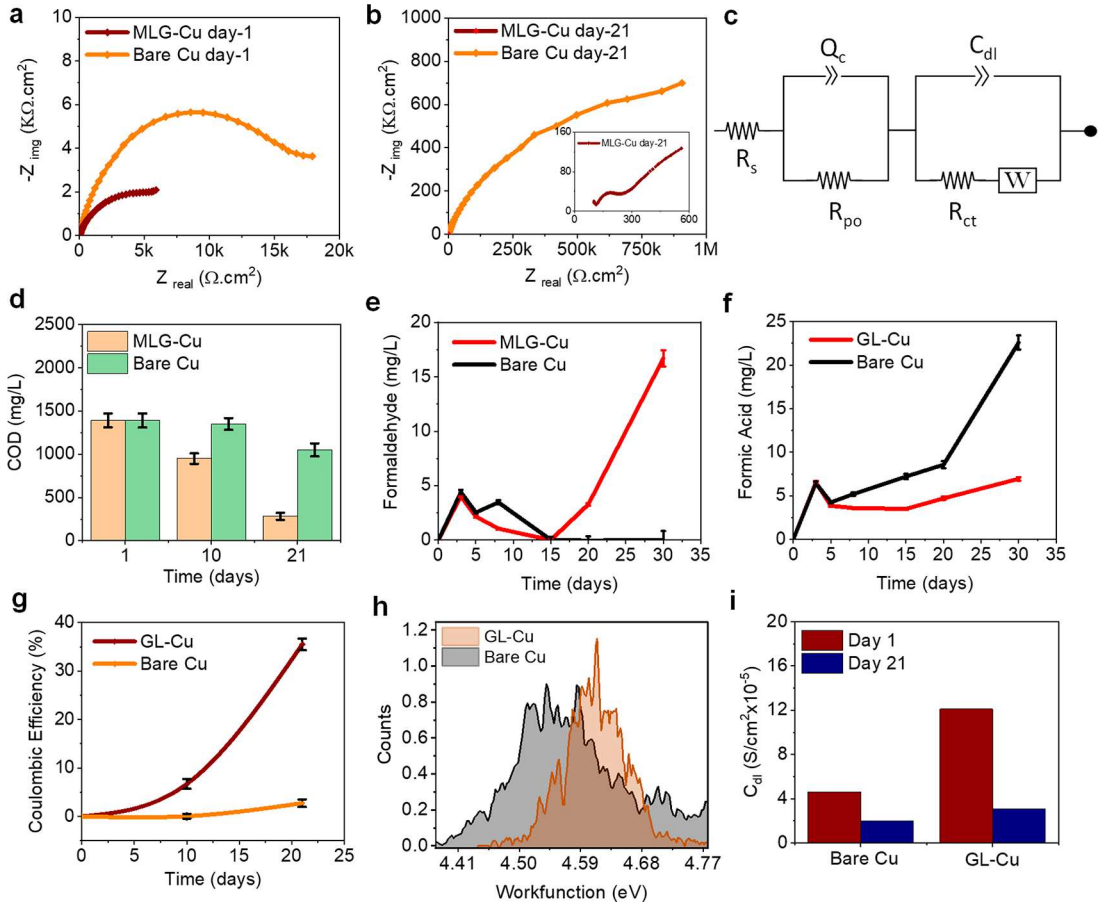

Figure 3. Measurement of electrochemical impedance (EIS). (a) GL-Cu and bare Cu on day 1 and (b) day 21. Electrical equivalent circuit (EEC) of (c) GL-Cu and Cu. Temporal profiles of (d) COD reduction, (e) formaldehyde, (f) formic acid, and (e) Coulombic efficiency. (h) Histogram of work function (WF, eV) distribution between unexposed Cu and GL-Cu; the ΔWF is measured ~60 meV, and (i) temporal profile of double layer capacitance.

compartment microbial fuel cell, Figure 2a, details in refs 37, 38). A genetically tractable *Rhodobacter sphaeroides* (Rsp) 2.4.1 served as a biocatalyst for facilitating CH_3OH dehydrogenation at the GL-Cu surfaces. Nitrate mineral salt (NMS) media modified with 0.1% CH_3OH served as an anolyte and 100 mM potassium ferricyanide in 50 mM phosphate buffer as a catholyte (details in the Methods Section). We assessed the use of pristine graphene layers on Cu electrodes for CH_3OH dehydrogenation using three different tests; they include (i) abiotic (GL-Cu), (ii) biotic (GL-Cu), and (iii) biotic (GL-GCE; GCE = glassy carbon electrode). All three tests used the same NMS media as an anolyte, except that the abiotic system was devoid of the Rsp cells.

CH_3OH-FC Performance in the Absence of Biocatalysts (Abiotic Conditions). The electrochemical behaviors of CH_3OH-FC for GL-Cu and bare-Cu were assessed and compared under abiotic conditions (Figure S4a–f). In the absence of the Rsp cells, the GL-Cu did not yield any noticeable current output from CH_3OH dehydrogenation in both tests (Figure S4b). The open circuit voltage (OCV) of GL-Cu (295 mV) under abiotic conditions (Figure S4a) was 2.4-fold lower than its biotic counterpart (681 mV, detailed in later sections). The CV for GL-Cu and bare Cu was also distinct, as shown in Figure S4c and d. The pseudopotential of 295 mV, primarily due to electrochemical double-layer capacitance, depleted rapidly upon the imposition of the external load (1000 Ω). The charge transfer resistance (R_{ct}) was 200-fold higher than biotic conditions, as measured from the electrochemical impedance spectroscopy (EIS) analysis (Figure S4e,f). These results confirm that the biocatalysts are needed to generate current from CH_3OH dehydrogenation. The lack of current also confirms that these abiotic conditions do not promote any galvanic coupling between Cu and graphene materials. These findings remained the same irrespective of the presence or absence of methanol in the anolyte (Figure S4a–f).

CH_3OH-FC Performance in Biotic Conditions. The graphene layers allow Rsp cells to sustain electrochemical current from the CH_3OH dehydrogenation on the Cu surfaces. Initially, we established the ability of the Gr layers to boost the electrocatalytic behavior of underlying Cu electrodes using a three-electrode electrochemical system with 50 mM potassium ferricyanide as an electrolyte. The current densities of GL-Cu were at least 2 orders of magnitude higher than the bare Cu system (cyclic voltammograms, Figure 2b). The remaining tests were carried out with the two-compartment CH_3OH-FCs discussed earlier. We measured and compared the voltage profiles of the GL-Cu and bare Cu under both open-circuit and closed-circuit conditions. The average OCV of the GL-Cu (681 mV) was 1.5-fold greater than bare Cu (430 mV; Figure 2c). The greater OCV values represent the higher potential for CH_3OH dehydrogenation. Next, we measured the voltage across an external resistor (R_{ext} = 1000 Ω) and the corresponding current density (obtained using Ohm's law)

https://doi.org/10.1021/acsnano.2c05512
ACS Nano 2023, 17, 137–145

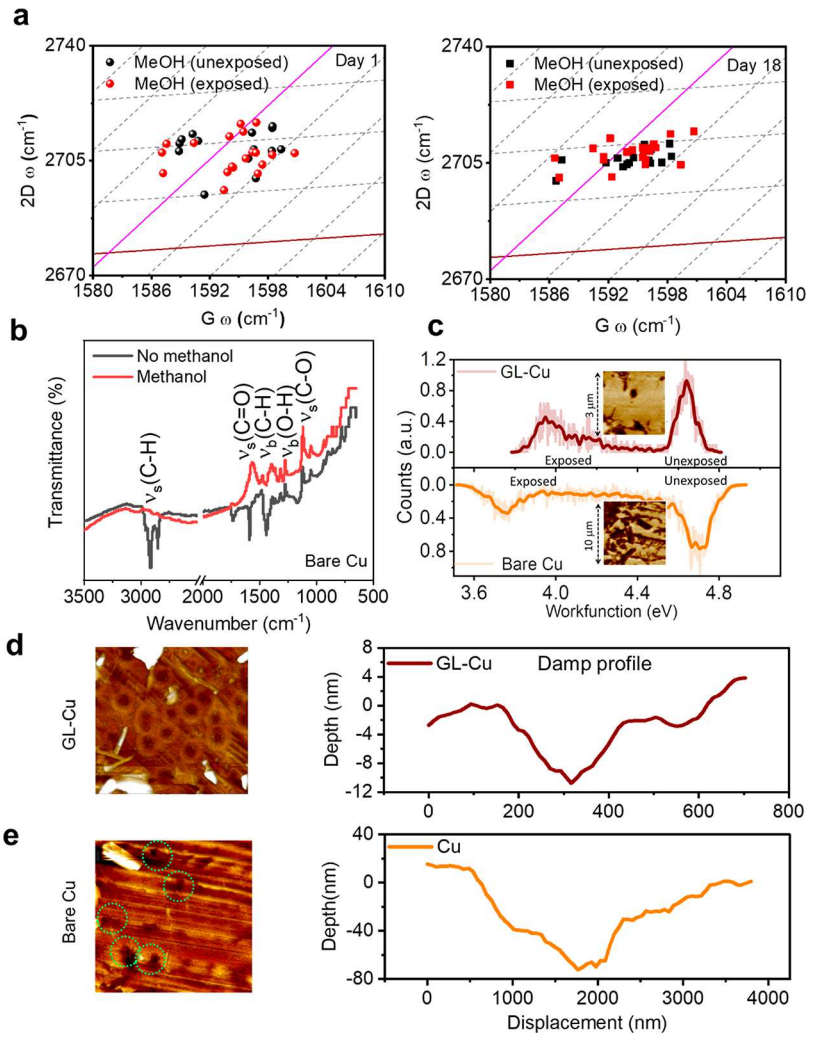

Figure 4. Enhanced surface interactions of methanol molecules by graphene nanolayers (a) distribution of Raman phonon modes (G, 2D) for GL-Cu at two different intervals (day 1 and day 18) after methanol exposure, (b) FTIR data on bare Cu, (c) comparison of surface potential bare Cu and GL-Cu for unexposed and exposed regions, and damp profile for (d) GL-Cu and (e) bare Cu for protection ability of GL against MeOH as compared to bare Cu.

under closed-circuit conditions (Figure 2d). The GL-Cu yielded 4 orders greater current density (895 mA/m^2) than bare Cu (0.305 mA/m^2). Higher current density confirms that the graphene layers boost the ability of Rsp cells to sustain current from the CH_3OH at the Cu surface (Figure 2d). The GL-Cu yielded reproducible performance over time, evident from the immediate restoration and sustenance of the current at a peak level after replacing 50% of the spent anolyte with the fresh NMS medium (Figure 2d). The superior behavior of the GL-Cu was evident even under polarized conditions, specifically under a varying external load (Figure 2e). The peak power density of GL-Cu (60 mW/m^2) was 60 000-fold higher than bare Cu (0.001 mW/m^2; Figure 2e). The results from the linear sweep voltammetry (LSV) corroborated that the GL-Cu yields a greater current density (4150 mA/m^2) than bare Cu. The latter was devoid of any dehydrogenation peaks (Figure 2f). Both the LSV tests were carried out on day 7 with a scan rate of 0.1 mV/s (Figure 2f).

The microscale imaging (5 × 5 μm^2) through conductive AFM revealed the differences in topography and current map between Cu and GL-Cu regions (Figure 2g). The bare Cu surface turned 4.7-fold rougher (Ra ≈ 18 nm) than the GL-coated surface (Ra ≈ 3.8 nm). This increase in roughness is due to the formation of a thin oxide layer that also disrupts the electrically conductive network due to an increase in resistance between the metallic tip apex and Cu surface. It is observed that the presence of the oxide layer decreases the current by 20%, which hampered the flow of current, as observed in the impedance behavior of Cu electrodes (Figure 3a).

We carried out electrochemical impedance spectroscopy (EIS) to assess the impact of the graphene layers on Faradaic reactions that influence methanol dehydrogenation on Cu electrodes. The R_{ct} for GL-Cu is 3.6-fold lower than bare Cu on day 1 (magnitude of a Nyquist arc, Figure 3a). The overall impedance for GL-Cu (R_{cell} = solution resistance (R_{soln}) + polarization resistance (R_{po}) + (R_{ct})) was 70% lower on day 1 and 99% lower on day 21 compared to bare Cu, respectively, based on the EEC fitting analysis (Figure 3a,b; Table S1). This phenomenal decline in the impedance corroborates that the GL promotes interactions among the Rsp cells and Cu surface for CH_3OH dehydrogenation (Table S2). The impedance spectra on both day 1 and day 21 followed a two-time constant model that connects R_s in series with the two-time constant components (Figure 3c). The first-time constant describes a

https://doi.org/10.1021/acsnano.2c05512
ACS Nano 2023, 17, 137−145

pore resistance (R_{po}) that accounts for conductive pathways for ions and electrons involved in CH_3OH dehydrogenation. The corresponding pore capacitance and accumulation of electrolytes at the graphene layers on the Cu are represented by the constant phase element (Q_c). The second-time constant describes the R_{ct} between Cu and the electrolyte and the capacitance due to the quantized double-layer phenomenon (Q_{dl}).

The CH_3OH consumption by the GL-Cu, measured in terms of chemical oxygen demand (COD), was 3.8-fold higher than bare Cu throughout the test duration (Figure 3d). GL-Cu yielded 3-fold higher levels of formaldehyde (Figure 3e) while reducing the undesirable accumulation of formic acid (Figure 3f). On the other hand, bare Cu consumed the formaldehyde, which would otherwise have been available to generate biomass and more electric current. As a result, the Coulombic efficiency (CE) of GL-Cu (37%) increased by 6-fold compared to bare Cu (~7%; Figure 3g). The GL-Cu displayed 2.6-fold higher double-layer capacitance than bare Cu, based on the EIS analysis (Figure 3i, Table S2). The investigation is extended to glassy carbon electrodes (GCE), a representative example of a nonmetallic electrode. The results reveal the benefit of graphene coating, owing to the structural similarities of GCE and graphene materials. The graphene layers facilitate bioelectrocatalytic dehydrogenation of CH_3OH on GCE (Figure S5a,b). The GL-GCE yielded ~1.2-fold higher OCV compared to bare GCE. The greater the OCV values, the higher the potential for CH_3OH dehydrogenation. These results are corroborated by a 605-fold higher current for GL-GCE than bare GCE, as shown in the $i-t$ curve (Figure S5 b).

Mechanisms of Bioelectrocatalytic Methanol Dehydrogenation on the Graphene Surfaces. After establishing that graphene layers boost the bioelectrocatalytic performance of copper electrodes, we used Kelvin probe force microscopy (KPFM) to investigate surface potential imaging of Cu and GL-Cu that translates into their work function (WF) behavior (details in the Methods Section). The presence of GL influences the localized WF (~60−80 meV) of underlying Cu surfaces[41] that can be observed by comparing Cu and GL-Cu prior to the exposure to CH_3OH (Figure 3h). It is worth noting that the thickness of graphene plays a crucial role as it relates to the electronic charge carriers that participate in the reaction. In our previous work, we demonstrated the formation of an electric double layer at the Cu−graphene interface in the electrolyte medium. The strength of the electrical double layer depends on the thickness of graphene over Cu. A fewer number of layers leads to higher strength in the electrical double layer and a lower WF and lower charge transfer resistance (R_{ct}). Thus, a higher number of graphene layers (>4 layers) is desirable. An example of variation in graphene surface potential at different thicknesses is measured over GL-Cu and GL-SiO_2 surfaces through Kelvin probe force microscopy (KPFM) in Figure S6a−f.

To monitor the role of thickness of GL sheets for surface charge distribution, a separate KPFM measurement has been conducted where thicker GL flakes (up to 120 nm height) were drop casted over bare Cu. The distribution of surface potential at different GL flakes reveals the increment of WF with a thickness indicating higher hole carriers at the topmost layer. Upon exposure to CH_3OH, GL-Cu experienced only a gradual change in WF (ΔWF = 0.7 eV) compared to an abrupt drop for bare Cu (ΔWF = 0.96 eV) with intermediate values of SLG-Cu (ΔWF = 0.96 eV) in Figure S6g. Furthermore, the GL-Cu surfaces resisted the strain and doping effects of CH_3OH, as observed from the overlapping Raman modes (G and 2D) for the exposed and unexposed regions, respectively. This phenomenon was apparent at both the beginning (day 1) and end of the tests (day 18; Figure 4a). This overlapping of Raman modes was also apparent in the deionized water system (Supporting Information, Figure S7). Compared to multilayered graphene, single-layered graphene failed to resist the straining effects (i.e., physical distortion) of CH_3OH, as observed from the compression in the C−C bonds for the SLG-Cu system (Figure S7a,b), thus justifying the use of multilayered graphene in this study.

The active role of graphene layers for promoting CH_3OH dehydrogenation by the Rsp cells on the Cu surfaces was validated through FTIR studies. The bare Cu displayed an intrinsic affinity for CH_3OH dehydrogenation,[48−50] which is evident from the FTIR signatures of formaldehyde and methoxy within 24 h of exposure to CH_3OH under ambient conditions (Figure 4b). This affinity was also reflected as modulation in the ΔWF when exposed to CH_3OH (surface potential micrographs, Figure 4c). Interestingly, GL preserved this intrinsic affinity of underlying Cu surfaces for CH_3OH, as observed through the ΔWF of the exposed Cu and GL-Cu surfaces, respectively (Figure 4c). The ΔWF remained unaltered when exposed to distilled water (control; Figure S8a−f). Despite the affinity of Cu surfaces for CH_3OH molecules, the bare Cu did not allow the Rsp cells to sustain current from the CH_3OH dehydrogenation (Figures 2 and 3). This confounding effect is due to the antimicrobial behavior of Cu. As seen in Figure S9, the protein content (an equivalent of cell density) for bare Cu (520 ± 17.7 μg/mL) was 1.5-fold lower than GL-Cu (760 ± 26.5 μg/mL) at the end of the tests.

Also, bare Cu underwent pitting corrosion that can be observed in the form of 60−75 nm deep pits, which were not apparent for GL-Cu (Figure 4d,e). Such corrosive effects result in the formation of undesirable oxidation species that discourage the overall extracellular electron transfer by the Rsp cells. The partially oxidized Cu species (e.g., Cu^+ or Cu^{2+}) within the oxide layers limit CH_3OH dehydrogenation and, in turn, reduce the accumulation of formate. For GL-Cu, graphene layers resisted anchoring of O_2 molecules onto the Cu surface[27] that discouraged undesirable oxidative scission (O−H bond) of CH_3OH into $CuOCH_3$ film[51] and subsequently minimized the formation of undesirable Cu-oxo species (e.g., $Cu(I)_S$ and $Cu(II)_{aq}$). Despite the large bond dissociation energy of O−H in CH_3OH (104.6 ± 0.7 kJ/mol) and C−H in CH_3O^- (104.99 ± 0.03 kJ/mol), respectively,[52] graphene layers promoted the CH_3OH dehydrogenation into formaldehyde (versus formate), encouraging the EET onto the GL-Cu via periplasmic c-type cytochromes. This formaldehyde reacts with tetrahydrofolate, allowing the Rsp cells to enter into the ribulose monophosphate (RuMP) or serine pathway to produce more biocatalysts (i.e., biomass). Additional tests confirmed the corrosion resistance of GL on Cu surfaces when exposed to two different types of oxidizing environments, including aggressive peroxide (30% H_2O_2, 2 h) and annealing (200 °C, 8 h) treatments, respectively (Figure S10). The exposure duration for these tests was selected based on the feedback from our earlier trials.[53]

CONCLUSIONS

We report the use of pristine graphene nanolayers as the thinnest, noninvasive coating for promoting catalyst-free

https://doi.org/10.1021/acsnano.2c05512
ACS Nano 2023, 17, 137−145

methanol dehydrogenation on copper electrodes in microbial methanol fuel cells. In addition to overcoming issues of material degradation and copper toxicity, graphene coatings retain the inherent work function behavior of underlying Cu surfaces toward methanol conversion into DC electricity. This study also highlights a need for obviating the use of single-layered graphene that promotes a compressive strain within carbon molecules of graphene coatings on Cu surfaces. The dual functions of the ultrathin graphene coatings, including passivation and bioelectrocatalytic behavior, can enable the use of metal electrodes in other bioelectrochemically driven batteries and supercapacitors.

METHODS

A brief account of experimental procedures is provided here, and comprehensive details are available in the Supporting Information. Graphene layers (GL) were conformally grown on 25-μm-thick copper foil using a low-pressure CVD at 1000 °C and 500 mTorr. A CH_4/H_2 mixture (10:30 sccm) was introduced at atmospheric pressure and 940 °C for 20 min. The GL was transferred onto glassy carbon electrodes using a PMMA transfer method. The CVD-grown GL on copper foil (Bare Cu electrode) is designated as GL-Cu and the glassy carbon electrode with the transferred film as GL-GCE.

A Gamry Reference 600 potentiostat was used to carry out both the direct current (DC) and alternate current (AC) electrochemistry tests. The electrochemical measurements were carried out only after allowing the system to reach steady-state open circuit voltage (OCV). Methanol fuel cells were modeled after a dual compartment fuel cell consisting of graphite felt as the cathode or counter electrode, the sample of the interest as the anode or working electrode, and Ag/AgCl as a reference electrode (RE). *Rhodobacter sphaeroides* 2.4.1 grown in the NMS media supplemented with 0.1% methanol serves as a biocatalyst.

Electrical equivalent circuits (EECs) were applied to the measured electrochemical impedance spectroscopy (EIS) data to determine ohmic resistance, polarization resistance, and charge transfer resistance of the stable electrochemical system. Atomic force microscopy (AFM)-Bruker Dimension Icon was used to carry out Kelvin probe force microscopy (KPFM) tests. Peak-force KPFM tests were performed using two pass modes: (i) collection of a topography image and (ii) the acquisition of potential map (contact potential difference, CPD). A conductive tip (Bruker Model: PFQNE-Al, stiffness $\approx 0.8 \pm 0.2$ N/m, diameter ≈ 5 nm, resonance frequency = 300 kHz) was used for the AFM measurements. The tip work function (WF) was carried out using freshly cleaved HOPG. The $WF_{sample} = WF_{tip} - eV_{dc}$ relation was used to determine the local WF values for Cu and GL-Cu exposed to 0.1% methanol.

The Raman spectroscopy was carried out with a 532 nm laser line and 1800 grating line/mm using the Renishaw inVia 100× optical lens. The laser power was limited to 5% (<1 mW) throughout the duration. The Raman peaks were fitted using the Lorentzian function to measure the peak positions for G and 2D peak. Raman spectroscopy, optical microscopy, scanning microscopy (SEM), atomic force microscopy (AFM), and contact angle measurements were carried out to determine the quality of graphene coatings. Prior to Raman, SEM, AFM, and optical microscopy tests, the graphene film was transferred onto a SiO_2/Si wafer using the PMMA transfer protocols.

ASSOCIATED CONTENT

Supporting Information

The Supporting Information is available free of charge at https://pubs.acs.org/doi/10.1021/acsnano.2c05512.

Optical, SEM, Raman spectroscopy, and contact angle analysis of Cu and GL-Cu; RSP inoculation and cultivation procedures; fuel cell experiments and electrochemical analysis, external equivalent circuit; methodology for transfer of graphene layers (GLs) onto SiO_2/Si; surface potentials map as a function of thickness and solvent exposure conditions (PDF)

AUTHOR INFORMATION

Corresponding Authors

Muhammad M. Rahman − *Department of Materials Science and Nanoengineering, Rice University, Houston, Texas 77005, United States;* orcid.org/0000-0003-1374-0561; Email: maksud@rice.edu

Pulickel M. Ajayan − *Department of Materials Science and Nanoengineering, Rice University, Houston, Texas 77005, United States;* orcid.org/0000-0001-8323-7860; Email: ajayan@rice.edu

Manoj Tripathi − *Department of Physics and Astronomy, University of Sussex, Brighton BN1 9RH, United Kingdom;* Email: m.tripathi@sussex.ac.uk

Rajesh Kumar Sani − *Department Civil and Environmental Engineering, South Dakota School of Mines and Technology, Rapid City, South Dakota 57701, United States; BuGReMeDEE Consortium, South Dakota School of Mines and Technology, Rapid City, South Dakota 57701, United States; 2Dimensional Materials for Biofilm Engineering Science and Technology (2DBEST) Center, South Dakota School of Mines and Technology, Rapid City, South Dakota 57701, United States;* orcid.org/0000-0002-5493-252X; Email: rajesh.sani@sdsmt.edu

Venkataramana Gadhamshetty − *Department Civil and Environmental Engineering, South Dakota School of Mines and Technology, Rapid City, South Dakota 57701, United States; BuGReMeDEE Consortium, South Dakota School of Mines and Technology, Rapid City, South Dakota 57701, United States; 2Dimensional Materials for Biofilm Engineering Science and Technology (2DBEST) Center, South Dakota School of Mines and Technology, Rapid City, South Dakota 57701, United States;* orcid.org/0000-0002-8418-3515; Email: venkata.gadhamshetty@sdsmt.edu

Authors

Jamil Islam − *Department Civil and Environmental Engineering, South Dakota School of Mines and Technology, Rapid City, South Dakota 57701, United States; BuGReMeDEE Consortium, South Dakota School of Mines and Technology, Rapid City, South Dakota 57701, United States*

Parthiba Karthikeyan Obulisamy − *Department Civil and Environmental Engineering, South Dakota School of Mines and Technology, Rapid City, South Dakota 57701, United States; BuGReMeDEE Consortium, South Dakota School of Mines and Technology, Rapid City, South Dakota 57701, United States*

Venkata K.K. Upadhyayula − *Department of Chemistry, Umeå University, SE 90187 Umeå, Sweden*

Alan B. Dalton − *Department of Physics and Astronomy, University of Sussex, Brighton BN1 9RH, United Kingdom;* orcid.org/0000-0001-8043-1377

Complete contact information is available at: https://pubs.acs.org/10.1021/acsnano.2c05512

Notes

The authors declare no competing financial interest.

https://doi.org/10.1021/acsnano.2c05512
ACS Nano 2023, 17, 137−145

ACKNOWLEDGMENTS

V.G. acknowledges the funding support from the National Science Foundation (NSF) awards (NSF CAREER, CBET-1454102; NSF, OIA-1736255; NSF OIA-1849206; NSF-1920954). M.T. and A.B.D. would like to acknowledge strategic development funding from the University of Sussex.

REFERENCES

(1) Feng, Y.; Liu, H.; Yang, J. A selective electrocatalyst-based direct methanol fuel cell operated at high concentrations of methanol. *Science advances* **2017**, *3* (6), No. e1700580.
(2) Samimi, F.; Rahimpour, M. R., Direct methanol fuel cell. In *Methanol*; Elsevier: 2018; pp 381−397.
(3) Kamarudin, S. K.; Achmad, F.; Daud, W. R. W. Overview on the application of direct methanol fuel cell (DMFC) for portable electronic devices. *International Journal of hydrogen energy* **2009**, *34* (16), 6902−6916.
(4) Huang, W.; Wang, H.; Zhou, J.; Wang, J.; Duchesne, P. N.; Muir, D.; Zhang, P.; Han, N.; Zhao, F.; Zeng, M.; Zhong, J.; Jin, C.; Li, Y.; Lee, S.-T.; Dai, H. Highly active and durable methanol oxidation electrocatalyst based on the synergy of platinum-nickel hydroxide-graphene. *Nat. Commun.* **2015**, *6* (1), 1−8.
(5) Rabissi, C.; Zago, M.; Grahl-Madsen, L.; Odgaard, M.; Casalegno, A. Local durability optimization of a large-scale direct methanol fuel cell: catalyst layer tuning for homogeneous operation and in-operando detection of localized hydrogen evolution. *J. Power Sources* **2021**, *506*, 230218.
(6) Carneiro, L. P.; Ferreira, N. S.; Tavares, A. P.; Pinto, A. M.; Mendes, A.; Sales, M. G. F. A passive direct methanol fuel cell as transducer of an electrochemical sensor, applied to the detection of carcinoembryonic antigen. *Biosens. Bioelectron.* **2021**, *175*, 112877.
(7) Lo Vecchio, C.; Serov, A.; Dicome, M.; Zulevi, B.; Arico, A.S.; Baglio, V. Investigating the durability of a direct methanol fuel cell equipped with commercial Platinum Group Metal-free cathodic electro-catalysts. *Electrochim. Acta* **2021**, *394*, 139108.
(8) Baruah, B.; Deb, P. Performance and Application of Carbon based Electrocatalysts in Direct Methanol Fuel Cell. *Materials Advances* **2021**, *2*, 5344−5364.
(9) Insider, L. Stationary Application definition. https://www.lawinsider.com/dictionary/stationary-application (accessed 12/05/2022).
(10) Store, F. C. Stationary Fuel Cell Power Applications. https://www.fuelcellstore.com/blog-section/stationary-fuel-cell-power-applications (accessed 12/05/2022).
(11) NAE NAE Grand Challenges for Engineering: 14 Grand Challenges for Engineering in the 21st Century http://www.engineeringchallenges.org/challenges.aspx (accessed 12/05/2022).
(12) Market, R. a. Direct Methanol Fuel Cells - Global Market Trajectory & Analytics. https://www.researchandmarkets.com/reports/5029966/direct-methanol-fuel-cells-global-market (accessed 12/05/2022).
(13) Administration, U. S. E. I. Energy use for transportation. https://www.eia.gov/energyexplained/use-of-energy/transportation.php (accessed 12/05/2022).
(14) Antolini, E. Formation of carbon-supported PtM alloys for low temperature fuel cells: a review. *Materials chemistry and physics* **2003**, *78* (3), 563−573.
(15) Jiang, L.; Sun, G.; Zhou, Z.; Zhou, W.; Xin, Q. Preparation and characterization of PtSn/C anode electrocatalysts for direct ethanol fuel cell. *Catal. Today* **2004**, *93*, 665−670.
(16) Liu, H.; Song, C.; Zhang, L.; Zhang, J.; Wang, H.; Wilkinson, D. P. A review of anode catalysis in the direct methanol fuel cell. *J. Power Sources* **2006**, *155* (2), 95−110.
(17) Strong, P. J.; Xie, S.; Clarke, W. P. Methane as a resource: can the methanotrophs add value? *Environ. Sci. Technol.* **2015**, *49* (7), 4001−4018.
(18) Semrau, A. L.; Stanley, P. M.; Urstoeger, A.; Schuster, M.; Cokoja, M.; Fischer, R. A. Substantial turnover frequency enhancement of MOF catalysts by crystallite downsizing combined with surface anchoring. *ACS Catal.* **2020**, *10* (5), 3203−3211.
(19) Besharat, Z.; Halldin Stenlid, J.; Soldemo, M.; Marks, K.; Önsten, A.; Johnson, M.; Öström, H.; Weissenrieder, J.; Brinck, T.; Göthelid, M. Dehydrogenation of methanol on Cu2O (100) and (111). *J. Chem. Phys.* **2017**, *146* (24), 244702.
(20) INSIDER Live Prices of Copper per ounce. https://markets.businessinsider.com/commodities/copper-price (accessed 12/05/2022).
(21) Baudler, A.; Schmidt, I.; Langner, M.; Greiner, A.; Schröder, U. Does it have to be carbon? Metal anodes in microbial fuel cells and related bioelectrochemical systems. *Energy Environ. Sci.* **2015**, *8* (7), 2048−2055.
(22) Kargi, F.; Eker, S. Electricity generation with simultaneous wastewater treatment by a microbial fuel cell (MFC) with Cu and Cu-Au electrodes. *Journal of Chemical Technology & Biotechnology: International Research in Process, Environmental & Clean Technology* **2007**, *82* (7), 658−662.
(23) Millo, D.; Harnisch, F.; Patil, S. A.; Ly, H. K.; Schröder, U.; Hildebrandt, P. In situ spectroelectrochemical investigation of electrocatalytic microbial biofilms by surface-enhanced resonance Raman spectroscopy. *Angew. Chem., Int. Ed.* **2011**, *50* (11), 2625−2627.
(24) Innovations, T. Metal Properties Table https://www.tibtech.com/conductivite (accessed 12/05/2022).
(25) Zuo, Z.-J.; Wang, L.; Han, P.-D.; Huang, W. Insights into the reaction mechanisms of methanol decomposition, methanol oxidation and steam reforming of methanol on Cu (111): A density functional theory study. *International journal of hydrogen energy* **2014**, *39* (4), 1664−1679.
(26) Bluhm, H.; Hävecker, M.; Knop-Gericke, A.; Kleimenov, E.; Schlögl, R.; Teschner, D.; Bukhtiyarov, V. I.; Ogletree, D. F.; Salmeron, M. Methanol oxidation on a copper catalyst investigated using in situ X-ray photoelectron spectroscopy. *J. Phys. Chem. B* **2004**, *108* (38), 14340−14347.
(27) Orozco, I.; Huang, E.; Mahapatra, M.; Shi, R.; Kang, J.; Nemsak, S.; Senanayake, S. D.; Liu, P.; Rodriguez, J. A. In Situ Studies of Methanol Decomposition Over Cu (111) and Cu2O/Cu (111): Effects of Reactant Pressure, Surface Morphology, and Hot Spots of Active Sites. *J. Phys. Chem. C* **2021**, *125* (1), 558−571.
(28) Zhu, X.; Logan, B. E. Copper anode corrosion affects power generation in microbial fuel cells. *J. Chem. Technol. Biotechnol.* **2014**, *89* (3), 471−474.
(29) Chilkoor, G.; Karanam, S. P.; Star, S.; Shrestha, N.; Sani, R. K.; Upadhyayula, V. K.; Ghoshal, D.; Koratkar, N. A.; Meyyappan, M.; Gadhamshetty, V. Hexagonal boron nitride: the thinnest insulating barrier to microbial corrosion. *ACS Nano* **2018**, *12* (3), 2242−2252.
(30) Zhao, F.; Slade, R. C.; Varcoe, J. R. Techniques for the study and development of microbial fuel cells: an electrochemical perspective. *Chem. Soc. Rev.* **2009**, *38* (7), 1926−1939.
(31) Narsimhan, K.; Iyoki, K.; Dinh, K.; Román-Leshkov, Y. Catalytic oxidation of methane into methanol over copper-exchanged zeolites with oxygen at low temperature. *ACS central science* **2016**, *2* (6), 424−429.
(32) Dumas, C.; Basseguy, R.; Bergel, A. Electrochemical activity of Geobacter sulfurreducens biofilms on stainless steel anodes. *Electrochim. Acta* **2008**, *53* (16), 5235−5241.
(33) Pons, L.; Délia, M.-L.; Basséguy, R.; Bergel, A. Effect of the semi-conductive properties of the passive layer on the current provided by stainless steel microbial cathodes. *Electrochim. Acta* **2011**, *56* (6), 2682−2688.
(34) Liu, Y.; Harnisch, F.; Fricke, K.; Sietmann, R.; Schröder, U. Improvement of the anodic bioelectrocatalytic activity of mixed culture biofilms by a simple consecutive electrochemical selection procedure. *Biosens. Bioelectron.* **2008**, *24* (4), 1006−1011.
(35) Yan, Y.; Shin, W. I.; Chen, H.; Lee, S.-M.; Manickam, S.; Hanson, S.; Zhao, H.; Lester, E.; Wu, T.; Pang, C. H. A recent trend: application of graphene in catalysis. *Carbon Letters* **2021**, *31* (2), 177−199.

https://doi.org/10.1021/acsnano.2c05512
ACS Nano 2023, 17, 137−145

(36) Wang, L.; Sofer, Z.; Pumera, M. Will any crap we put into graphene increase its electrocatalytic effect? *ACS Nano* **2020**, *14* (1), 21−25.
(37) Islam, J.; Chilkoor, G.; Jawaharraj, K.; Dhiman, S. S.; Sani, R.; Gadhamshetty, V. Vitamin-C-enabled reduced graphene oxide chemistry for tuning biofilm phenotypes of methylotrophs on nickel electrodes in microbial fuel cells. *Bioresource technology* **2020**, *300*, 122642.
(38) Jawaharraj, K.; Sudha Dhiman, S.; Bedwell, S.; Vemuri, B.; Islam, J.; Sani, R. K.; Gadhamshetty, V. Electricity from methane by Methylococcus capsulatus (Bath) and Methylosinus trichosporium OB3b. *Bioresour. Technol.* **2021**, *321*, 124398.
(39) Jawaharraj, K.; Shrestha, N.; Chilkoor, G.; Dhiman, S. S.; Islam, J.; Gadhamshetty, V. Valorization of methane from environmental engineering applications: A critical review. *Water Res.* **2020**, *187*, 116400.
(40) Kim, K. K.; Hsu, A.; Jia, X.; Kim, S. M.; Shi, Y.; Dresselhaus, M.; Palacios, T.; Kong, J. Synthesis and characterization of hexagonal boron nitride film as a dielectric layer for graphene devices. *ACS Nano* **2012**, *6* (10), 8583−8590.
(41) Chilkoor, G.; Shrestha, N.; Kutana, A.; Tripathi, M.; Robles Hernandez, F. C.; Yakobson, B. I.; Meyyappan, M.; Dalton, A. B.; Ajayan, P. M.; Rahman, M. M.; Gadhamshetty, V. Atomic Layers of Graphene for Microbial Corrosion Prevention. *ACS Nano* **2021**, *15* (1), 447−454.
(42) Ni, Z.; Wang, H.; Kasim, J.; Fan, H.; Yu, T.; Wu, Y. H.; Feng, Y.; Shen, Z. Graphene thickness determination using reflection and contrast spectroscopy. *Nano Lett.* **2007**, *7* (9), 2758−2763.
(43) Lu, J. P. Elastic properties of carbon nanotubes and nanoropes. *Physical review letters* **1997**, *79* (7), 1297.
(44) Hsieh, Y.-P.; Hofmann, M.; Chang, K.-W.; Jhu, J. G.; Li, Y.-Y.; Chen, K. Y.; Yang, C. C.; Chang, W.-S.; Chen, L.-C. Complete corrosion inhibition through graphene defect passivation. *ACS Nano* **2014**, *8* (1), 443−448.
(45) Kirkland, N.; Schiller, T.; Medhekar, N.; Birbilis, N. Exploring graphene as a corrosion protection barrier. *Corros. Sci.* **2012**, *56*, 1−4.
(46) Tripathi, M.; Lee, F.; Michail, A.; Anestopoulos, D.; McHugh, J. G.; Ogilvie, S. P.; Large, M. J.; Graf, A. A.; Lynch, P. J.; Parthenios, J.; Papagelis, K.; Roy, S.; Saadi, M. A. S. R.; Rahman, M. M.; Pugno, N. M.; King, A. A. K.; Ajayan, P. M.; Dalton, A. B. Structural defects modulate electronic and nanomechanical properties of 2D materials. *ACS Nano* **2021**, *15* (2), 2520−2531.
(47) Rafiee, J.; Mi, X.; Gullapalli, H.; Thomas, A. V.; Yavari, F.; Shi, Y.; Ajayan, P. M.; Koratkar, N. A. Wetting transparency of graphene. *Nature materials* **2012**, *11* (3), 217−222.
(48) Daiyan, R.; Lu, X.; Ng, Y. H.; Amal, R. Liquid Hydrocarbon Production from CO2: Recent Development in Metal-Based Electrocatalysis. *ChemSusChem* **2017**, *10* (22), 4342−4358.
(49) Gattrell, M.; Gupta, N.; Co, A. A review of the aqueous electrochemical reduction of CO2 to hydrocarbons at copper. *Journal of electroanalytical Chemistry* **2006**, *594* (1), 1−19.
(50) Lee, S.; Lee, J. Electrode Build-Up of Reducible Metal Composites toward Achievable Electrochemical Conversion of Carbon Dioxide. *ChemSusChem* **2016**, *9* (4), 333−344.
(51) Banaś, J.; Stypuła, B.; Banaś, K.; Światowska-Mrowiecka, J.; Starowicz, M.; Lelek-Borkowska, U. Corrosion and passivity of metals in methanol solutions of electrolytes. *J. Solid State Electrochem.* **2009**, *13* (11), 1669.
(52) Nimlos, M. R.; Blanksby, S. J.; Ellison, G. B.; Evans, R. J. Enhancement of 1, 2-dehydration of alcohols by alkali cations and protons: a model for dehydration of carbohydrates. *Journal of analytical and applied pyrolysis* **2003**, *66* (1−2), 3−27.
(53) Chen, S.; Brown, L.; Levendorf, M.; Cai, W.; Ju, S.-Y.; Edgeworth, J.; Li, X.; Magnuson, C. W.; Velamakanni, A.; Piner, R. D.; Kang, J.; Park, J.; Ruoff, R. S. Oxidation resistance of graphene-coated Cu and Cu/Ni alloy. *ACS Nano* **2011**, *5* (2), 1321−1327.

https://doi.org/10.1021/acsnano.2c05512
ACS Nano 2023, 17, 137−145